Magnetic Resonance Imaging 33 (2015) 816–821

Contents lists available at ScienceDirect

Magnetic Resonance Imaging

journal homepage: www.mrijournal.com

Brain morphology is individual-specific information

Hidemasa Takao [a,*], Naoto Hayashi [b], Kuni Ohtomo [a]

[a] Department of Radiology, Graduate School of Medicine, University of Tokyo, 7-3-1 Hongo, Bunkyo-ku, Tokyo, Japan
[b] Department of Computational Diagnostic Radiology and Preventive Medicine, Graduate School of Medicine, University of Tokyo, 7-3-1 Hongo, Bunkyo-ku, Tokyo, Japan

ARTICLE INFO

Article history:
Received 22 February 2015
Accepted 30 March 2015

Keywords:
Biometrics
Brain morphology
Eigenbrain
Magnetic resonance imaging
Recognition
Voxel-based morphometry

ABSTRACT

The identification of individual differences in brain morphology is important to understand the background of individual differences in brain functions. In the present study, we investigated whether brain morphology is discernibly different among individuals and is personally identifiable information. Using structural magnetic resonance imaging data from 215 healthy subjects scanned twice (scan interval = 1.0 ± 0.1 years), we performed brain recognition by image normalization using a voxel-based morphometry approach, feature extraction based on principal component analysis, and calculating the Euclidean distances between image pairs projected into the subspace. Even with only 32 dimensions used for projection, the rank-one identification rate was 99.5%. With ≥112 dimensions used, the rank-one identification rate was 100%. At a false accept rate of 0.01%, the genuine accept rates were 95.8% and 100% with 32 and ≥128 dimensions used for projection, respectively. There was little difference in the Euclidean distances among different combinations of scanners used or between probe–gallery image pairs with and without scanner upgrade. These results indicate that brain morphology can identify a specific individual; i.e., brain morphology is personally identifiable information. Individually different brain morphology may occur as a collection of differences in brain structures that reflect individual differences in a variety of performances and various psychological characteristics and behavior patterns, and may provide the background of individual differences in personality and brain function.

1. Introduction

To understand the background of individual differences in brain functions, it is important to identify individual differences in brain morphology. Brain morphology is the study of the size and shape of the brain and its structures. With recent advances in magnetic resonance imaging (MRI) and image analysis techniques, brain morphometry has been widely used to study brain structures and their differences in normal brains, in developing and aging brains, and in a variety of neurological and neuropsychiatric disorders. Structural changes occur during brain development, maturation, and aging that are related to changes in brain functions. Moreover, a variety of neurological and neuropsychiatric disorders cause and/or are related to changes in brain structures. In addition to its association with brain development and aging, as well as neurological and neuropsychiatric disorders, brain morphology is also related to various types of high-level performance such as those displayed by taxi drivers [1], musicians [2,3], mathematicians [4], and bilingual individuals [5]. Even learning and training have been shown to cause changes in brain structures [6]. In addition, brain morphometry has been performed to investigate the relationship of brain structures to a wide range of personality dimensions and behavioral traits. Morphometric changes in the brain manifest as a gain or loss of brain tissue, which can be detected by structural MRI. Most typically, T1-weighted images are used for morphometric analysis of the brain with MRI.

Techniques for morphometric analysis of these brain images include visual assessment, manual tracing of regions of interest, and automated methods such as voxel-based morphometry (VBM) [7]. Manual tracing of regions of interest is a widely used form of brain morphometry; however, it is a subjective and time-consuming procedure, requires considerable anatomical expertise, and is generally limited to brain structures that have constant anatomical boundaries. Recently, a number of automated, unbiased, objective techniques have been developed and widely used to examine brain morphology, including volume-based methods such as VBM [7], tensor-based morphometry, and deformation-based morphometry; and surface-based methods such as cortical thickness analysis. VBM is one of the most commonly used automated techniques for assessing brain structures. Briefly, VBM involves segmenting images into gray matter, white matter, and cerebrospinal fluid; warping these tissue maps into standard space; smoothing these spatially normalized tissue maps; before performing voxel-by-voxel statistical analysis.

* Corresponding author at: Department of Radiology, Graduate School of Medicine, University of Tokyo, 7-3-1 Hongo, Bunkyo-ku, Tokyo 113–8655, Japan.Tel.: +81 3 5800 8666; fax: +81 3 5800 8935.
E-mail address: takaoh-tky@umin.ac.jp (H. Takao).

http://dx.doi.org/10.1016/j.mri.2015.03.010
0730-725X/

Recently, large-scale brain imaging studies have been conducted to overcome the limited power of smaller studies and to increase reliability of the findings. These studies include the Alzheimer's Disease Neuroimaging Initiative study [8], a multi-center observational study of healthy elders and patients with mild cognitive impairment and Alzheimer's disease; and the Human Connectome Project [9], a project to construct a map of the complete structural and functional neural connections in vivo within and across healthy individuals. These large-scale brain imaging studies have made "de-identified" data, including imaging and clinical information and DNA sequences, widely available to the scientific community for examination and exploration.

The recent proliferation of digital networks and the growth of the information society have further enhanced the need for information security and reliable personal identification. Biometrics use physical characteristics such as fingerprints, iris properties, and face extraction to establish the identity of a person. The unique nature of the fingerprint is one of the most well-known and commonly used biometric traits. Fingerprint recognition has been in use for over a century and has recently become automated following advances in computer technology. In contrast, humans most commonly recognize individuals on the basis of facial features. Although automated face recognition by computers has improved, this method is more difficult than automated fingerprint recognition, and the need for a high-accuracy system remains.

In the present study, we investigated whether brain morphology is discernibly different among individuals and is personally identifiable information. Using structural MRI data from 215 healthy subjects who were scanned twice, for this purpose, we performed brain recognition by image normalization using the VBM approach [10], feature extraction based on principal component analysis (PCA), and calculation of the Euclidean distances between image pairs in the subspace.

2. Materials and methods

2.1. Subjects

The present study included data from 215 healthy subjects (153 males, 62 females, mean age = 56 ± 9 years, age range = 40–83 years) [11]. None of the subjects had a history of neuropsychiatric disorders, including serious head trauma, psychiatric disorder, or alcohol/substance abuse or dependence. The mean mini-mental state examination score was 29.6 ± 0.7 (range = 27–30). A board-certified radiologist reviewed all scans including T1-weighted and T2-weighted images and found no gross abnormalities such as infarct, hemorrhage, or brain tumor in any subject. Fazekas score (range, 0–3) was 0 (absence) or 1 (caps, pencil-thin lining and/or punctate foci) [12]. The Ethical Committee of the University of Tokyo Hospital approved the study. After a complete explanation of the study to each subject, written informed consent was obtained.

2.2. Imaging data acquisition

Magnetic resonance data were obtained on two 3.0-T Signa scanners (GE Medical Systems, Milwaukee, WI) with an 8-channel brain phased-array coil. The scanners were the exact same model, and were simultaneously upgraded from HDx to HDxt. Each subject was scanned twice, at an interval of about 1 year (mean interval = 1.0 ± 0.1 years, range = 0.6–1.3 years) [11]. Of the 215 subjects, (A) 67 were scanned twice with scanner 1; (B) 44 were first scanned with scanner 1 and then with scanner 2; (C) 56 were first scanned with scanner 2 and then with scanner 1; and (D) the remaining 48 were scanned twice with scanner 2. Of the 215 subjects, 151 underwent both scans before scanner upgrade, and the remaining 64 underwent the first scan before upgrade and the second after the upgrade.

T1-weighted images were acquired using three-dimensional inversion recovery prepared fast spoiled gradient recalled acquisition in the steady state in 176 sagittal slices (repetition time = 5.3–5.4 ms; echo time = 1.7 ms; inversion time = 450 ms; flip angle = 15°; field of view = 250 mm; slice thickness = 1.0 mm with no gap; acquisition matrix = 256 × 256; number of excitations = 0.5; image matrix = 256 × 256). Parallel imaging (array spatial sensitivity encoding technique) was used with an acceleration factor of 2.0. Voxel dimensions were 0.977 mm × 0.977 mm × 1.0 mm. The images were corrected for spatial distortion due to gradient non-linearity using grad_unwarp [13–15] and for intensity non-uniformity using the nonparametric non-uniform intensity normalization algorithm N3 [14–16].

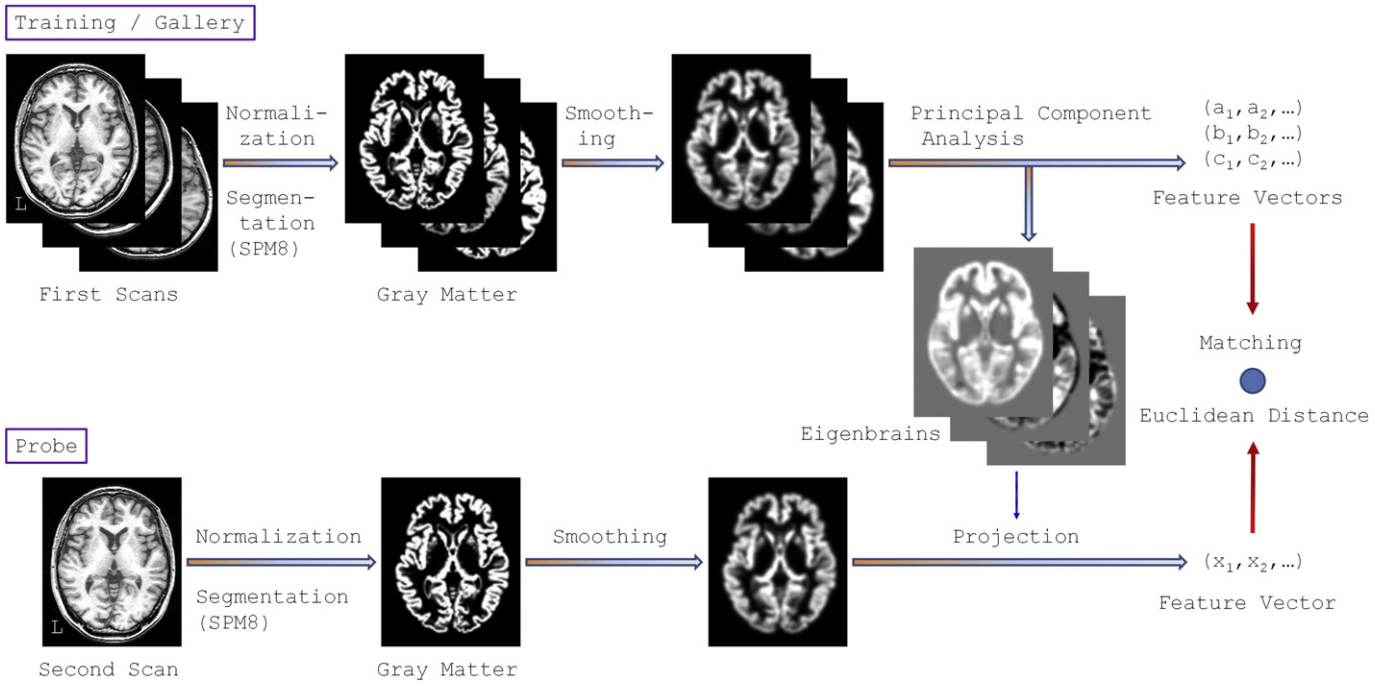

Fig. 1. Summary of image processing for brain recognition using PCA.

2.3. PCA-based brain recognition

Image processing was performed mainly using MATLAB 7.13 (Mathworks, Sherborn, MA) and statistical parametric mapping 8 software (http://www.fil.ion.ucl.ac.uk/spm) developed in the Wellcome Department of Imaging Neuroscience, Institute of Neurology, University College London.

The first scans were used as a training and gallery set and the second scans were used as a probe set. Fig. 1 shows a summary of image processing steps. All images were normalized using unified segmentation [10] implemented in statistical parametric mapping 8 software (VBM approach). The "eigenbrain" space was created using PCA on the normalized training images. Recognition was performed by calculating the distances from the probe to gallery images projected into the eigenbrain space.

2.3.1. Image normalization

The inversion recovery prepared fast spoiled gradient recalled acquisition in the steady state images were spatially normalized and segmented into gray matter, white matter, and cerebrospinal fluid using an integrated generative model (unified segmentation) [10]. The International Consortium for Brain Mapping gray matter, white matter, and cerebrospinal fluid templates were used as priors to segment the images. The normalized gray matter images were modulated to correct voxel signal intensity for volume displacement during normalization and reflect brain volume [17], smoothed by an isotropic Gaussian kernel (sigma = 2 mm). The final voxel size was 2 mm × 2 mm × 2 mm.

2.3.2. Principal component analysis

The mean image *m* was calculated and subtracted from the normalized training images. We performed PCA to determine eigenvectors v_1, v_2, …, v_{n-1} ("eigenbrains"), where *n* is the number of the training images (215). The dimensions were reduced to decrease the number of eigenbrains used while minimizing the loss of information by keeping those eigenbrains with the largest eigenvalues. Each (mean-subtracted) image can be projected into this space and the projected image is represented as a weighted sum of the eigenbrains. The weight vector (feature vector) represents the position of the brain in this space and is the result of the projection.

2.3.3. Recognition

Recognition was performed by projecting a probe image into the eigenbrain space, and comparing it with the gallery images projected into the eigenbrain space by measuring the Euclidean distances between their respective feature vectors.

3. Results

3.1. Eigenbrains and variance explained

Fig. 2 shows the mean image and eigenbrains calculated from the training (gallery) set. Fig. 3 shows the cumulative percentages of variance explained by the principal components (eigenbrains). Of the 214 principal components (eigenbrains) calculated, the first 21, 38, 60, 86, 119, and 159 principal components (eigenbrains) explained 40%, 50%, 60%, 70%, 80%, and 90% of the total variance, respectively.

3.2. Euclidean distances and dimensions used

Fig. 4 and Table 1 show the relationship between the number of dimensions (eigenbrains) used and Euclidean distances between the probe and gallery images. As the number of dimensions (eigenbrains) used increased, the distances from the others increased, while the distances from oneself were almost stable. Even with a small number of dimensions (eigenbrains) used, the distances from the others were sufficiently long compared with the distances from oneself.

3.3. Identification and dimensions used

Fig. 5 shows the relationship between the number of dimensions (eigenbrains) used and the rank-one identification rate. The gallery image with the smallest Euclidean distance from a probe image is the top (rank-one) match. When 16, 32, 48, 64, 80, 96, and 112 dimensions (eigenbrains) were used for projection, the rank-one identification rates were 97.2% (209/215), 99.5% (214/215), 99.5%, 99.5%, 99.5%, 99.5%, and 100% (215/215), respectively.

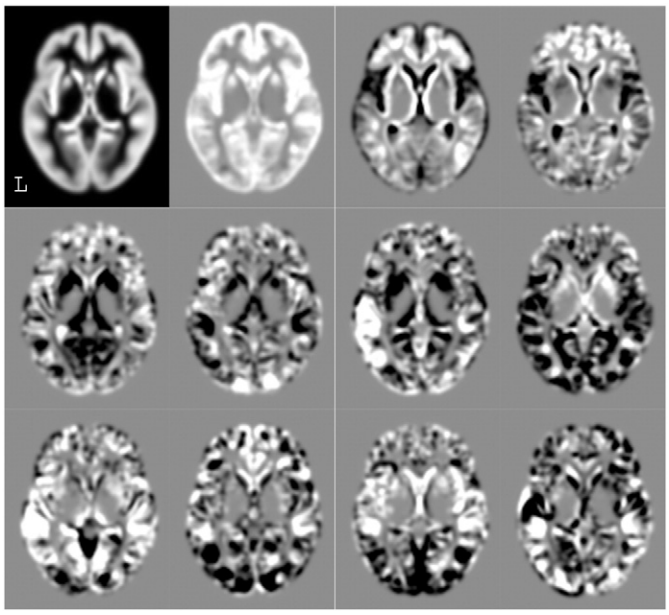

Fig. 2. Mean image and the first 11 eigenbrains calculated from the training (gallery) set.

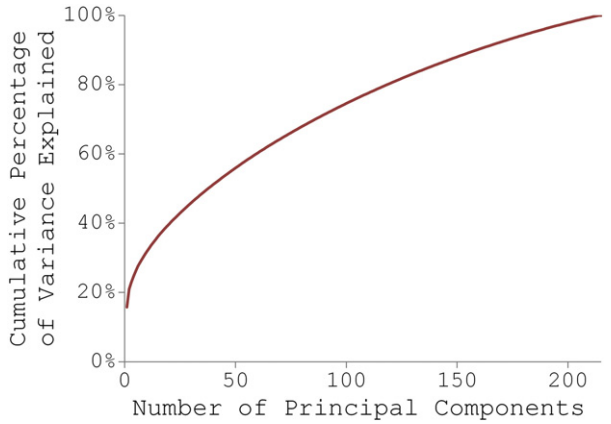

Fig. 3. Cumulative percentage of variance explained by the principal components (eigenbrains).

3.4. Verification and dimensions used

Matching all the probe images (n = 215) against all the gallery images (n = 215) yielded 215 genuine scores (Euclidean distances) (where images are from the same subject) and 215 × 214 (46,010) imposter scores (Euclidean distances) (where images are from different subjects). Fig. 6 shows receiver operating characteristic curves calculated with different numbers of dimensions (eigenbrains) used for projection. When 16 dimensions (eigenbrains) were used, the genuine accept rates were 89.8% and 82.8% at false accept rates of 0.01% and 0.001%, respectively. When 32 dimensions (eigenbrains) were used, the genuine accept rates were 95.8% and 90.7%, at false accept rates of 0.01% and 0.001%, respectively. When 48 dimensions (eigenbrains) were used, the genuine accept rates were 98.1% and 97.2% at false accept rates of 0.01% and 0.001%, respectively. When 64 dimensions (eigenbrains) were used, the genuine accept rates were 98.6% and 98.6% at false accept rates of 0.01% and 0.001%, respectively. When 80, 96, or 112 dimensions (eigenbrains) were used, the genuine accept rates were 99.1% and 99.1% at false accept rates of 0.01% and 0.001%, respectively. When 128 dimensions (eigenbrains) were used, the genuine accept rates were 100% and 99.1% at false accept rates of 0.01% and 0.001%, respectively. When 144 dimensions (eigenbrains) were used, the genuine accept rates were 100% and 99.5% at false accept rates of 0.01% and 0.001%, respectively. When 160 dimensions (eigenbrains) were used, the genuine accept rates were 100% and 100% at false accept rates of 0.01% and 0.001%, respectively.

Table 1
Euclidean distances between the probe and gallery images.

	Number of dimensions (eigenbrains) used													
	16	32	48	64	80	96	112	128	144	160	176	192	208	214
Distance from oneself														
Mean	8	8	9	9	9	9	9	9	10	10	10	10	10	10
SD	4	4	4	4	4	4	4	4	4	4	4	4	4	4
Distance from the nearest other														
Mean	18	24	29	32	35	37	39	41	43	45	46	48	50	51
SD	4	6	7	7	8	8	8	8	8	8	8	7	6	5
Distance from the others														
Mean	37	42	45	48	51	53	54	56	57	59	60	61	62	62
SD	12	11	11	11	11	11	10	10	10	9	9	9	8	8
Difference between the distance from oneself and that from the nearest other														
Mean	10	16	20	23	25	28	30	31	33	35	37	38	40	41
SD	5	7	8	8	9	9	9	9	9	9	9	8	7	7
p^*	All p values were < 0.0001.													

* - Wilcoxon signed-rank test

3.5. Effects of scanner and upgrade

Figs. 7 and 8 show the effects of using different scanners and of scanner upgrade on the Euclidean distances calculated between the probe and gallery images. There was little difference in the Euclidean distances among the different combinations of scanners used or between the probe–gallery image pairs with and without scanner upgrade.

4. Discussion

The results of the present study indicate that brain morphology can identify a specific individual; i.e., brain morphology is personally identifiable information. Even with only 32 dimensions (eigenbrains) used for projection, the rank-one identification rate was 99.5%. The rank-one identification rate was 100% with ≥112 dimensions (eigenbrains) used. At a false accept rate of 0.01%, the genuine accept rates were 95.8% and 100% with 32 and ≥128 dimensions (eigenbrains) used for projection, respectively. Brain morphology undergoes change during brain development, maturation, and aging. Moreover, a variety of neurological and neuropsychiatric disorders cause and/or are related to changes in brain morphology. In addition, previous studies have reported a relationship between brain structures and various types of high-level performance, and even personality dimensions and behavioral traits. Individual differences in brain morphology may occur as a collection of differences in brain structures

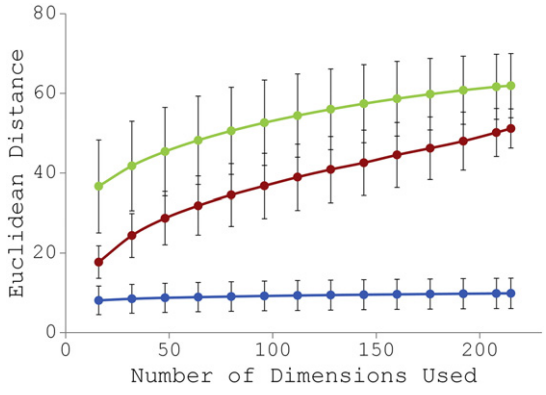

Fig. 4. Euclidean distances between the probe and gallery images. Blue dots are the distances from oneself, red dots are the distances from the nearest other, and green dots are the distances from all the others. The error bars represent the standard deviation.

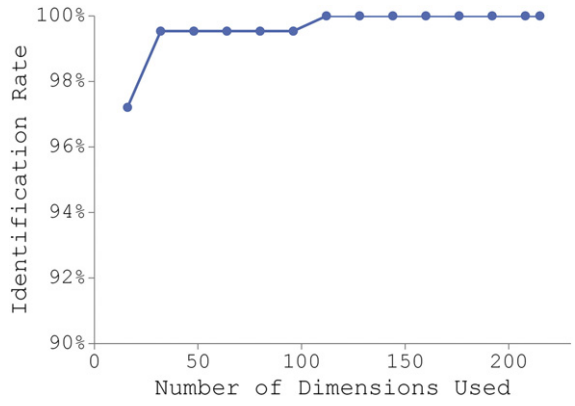

Fig. 5. Rank-one identification rate. When 16, 32 (48, 64, 80, 96), and 112 dimensions (eigenbrains) were used for projection, the rank-one identification rates were 97.2%, 99.5%, and 100%, respectively.

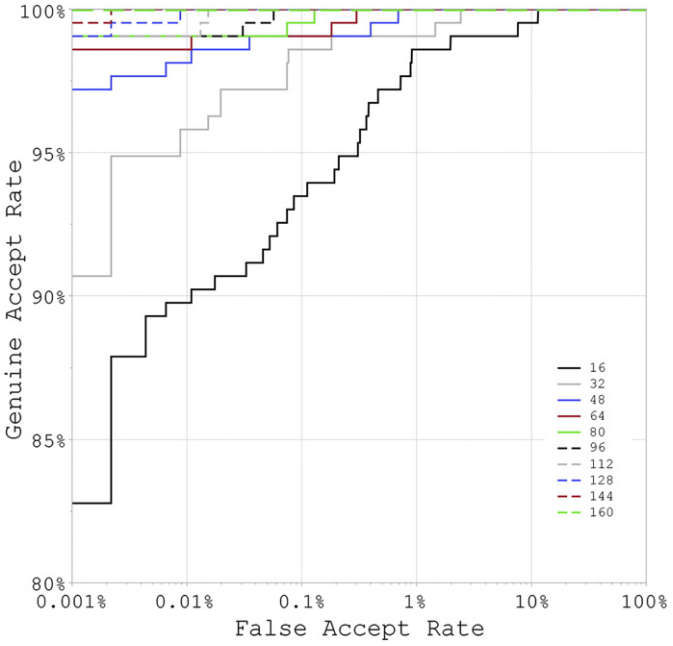

Fig. 6. Receiver operating characteristic curves. At a false accept rate of 0.01%, the genuine accept rates were 89.8%, 95.8%, 98.1%, 98.6%, 99.1%, 99.1%, 99.1%, 100%, 100%, and 100% with 16, 32, 48, 64, 80, 96, 112, 128, 144, and 160 dimensions (eigenbrains) used for projection, respectively. At a false accept rate of 0.001%, the genuine accept rates were 82.8%, 90.7%, 97.2%, 98.6%, 99.1%, 99.1%, 99.1%, 99.1%, 99.5%, and 100%, respectively.

that reflect individual differences in a variety of performances and various psychological characteristics and behavior patterns, and may provide the background of individual differences in personality and brain function.

To our knowledge, few previous studies have evaluated inter-individual differences in brain morphology from the point of view of biometrics [18–20]. Aloui et al. reported preliminary results of brain recognition using a single slice of structural MRI [18,19]. Chen et al. performed brain recognition using image normalization and a simple pixel-level matching method [20] or gray matter extraction and Chamfer matching. Chen et al. reported results collected using structural MRI data obtained from the Open Access Series of Imaging Studies database [21,22], which consists of non-demented and demented subjects, including patients with mild to moderate Alzheimer's disease, who thus had larger inter-subject variability in brain morphology compared with healthy subjects.

For the purpose of demonstrating the possibility of brain morphology as personally identifiable information, in the present study, we used VBM [7] for image normalization and PCA for feature extraction. Despite the relative simplicity of this method, it was possible to identify a specific individual on the basis of structural MRI of the brain. Brain morphology is three-dimensional information and that is richer in information compared with other biometrics such as fingerprints, iris patterns, and face recognition. If the method for brain recognition becomes more sophisticated like those used for recognition of these other biometrics (which itself is out of the main scope of the present study), brain recognition will become more accurate and precise. Recent large-scale brain imaging studies, such as the Alzheimer's Disease Neuroimaging Initiative study [8] and the Human Connectome Project [9] have made de-identified data, including imaging and clinical information and DNA sequences, widely available to the scientific community. However, images of the brain also include personally identifiable information. It is necessary to handle data with careful attention. On the other hand, in a clinical setting such as a hospital, brain recognition can be applied for verifying a patient's identity, preventing patients' imaging data from being erroneously confused, or for other potential applications in the future.

The brain rapidly grows during early development, the changes become more subtle during maturation and aging, and the brain gradually atrophies with aging. Brain atrophy accelerates with increasing age and the observed rate varies according to the age range of the studied sample [23]. Annual atrophy rates vary across the cortex, but are typically ~0.5% in the aged [24]. Atrophy in patients with Alzheimer's disease is much more rapid than in normal individuals, with most areas showing an annual atrophy rate of 1% or more [24]. As gallery and probe data sets, in the present study, we used structural MRI data from 215 healthy subjects scanned twice at an interval of about 1 year, and achieved successful brain recognition. We consider that this result was due to inter-subject variability in brain morphology being much larger than 1-year change in brain structures. Excluding the principal component (eigenbrain) related to aging from brain recognition may enable successful brain recognition, even for data pairs with a much longer scan interval.

Many previous studies have evaluated the effects of using different scanners and/or scanner upgrade on morphometric results [11,25–38]. Regarding volumetric measurements, there is generally greater inter-scanner variability than intra-scanner variability. Even with scanners of the exact same model, the use of different scanners

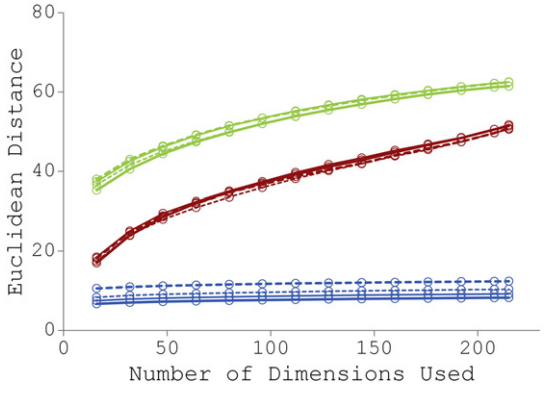

Fig. 7. Euclidean distances between the probe and gallery images for each combination of scanners used (A–D). Blue dots are the distances from oneself, red dots are the distances from the nearest other, and green dots are the distances from all the others (A = thick line, B = thick dotted line, C = thin dotted line, D = thin line).

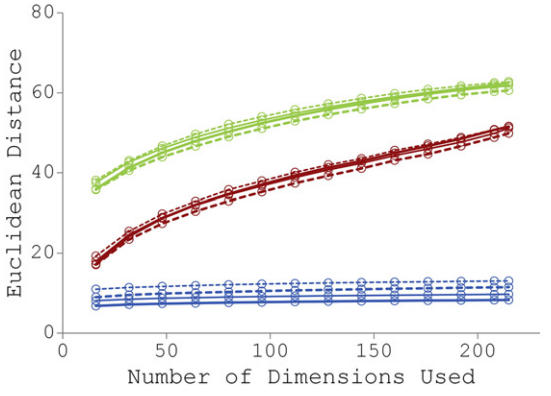

Fig. 8. Euclidean distances between the probe and gallery images for probe–gallery image pairs with and without scanner upgrade. Blue dots are the distances from oneself, red dots are the distances from the nearest other, and green dots are the distances from the others (without and with upgrade of scanner 1 = thick line and thick dotted line; without and with upgrade of scanner 2 = thin line and thin dotted line).

can influence morphometric results, and scanner upgrade can also have effects comparable to those of the use of different scanners (of the exact same model) [11,37]. In the present study, we used grad_unwarp and N3 to correct for geometric distortion due to gradient non-linearity and intensity non-uniformity, respectively. Intensity non-uniformity is caused by factors such as inhomogeneous radiofrequency fields, inhomogeneous reception sensitivity, and electromagnetic interaction with the object being scanned [39]. Grad_unwarp corrects for geometric distortion caused by gradient non-linearity but not that caused by scanner-dependent geometrical inaccuracies. It is impossible to completely eliminate scanner effects themselves, which are considered inevitable to a greater or lesser extent [11,37].

In the present study, we used structural imaging data obtained on two MRI scanners of the exact same model. Each subject was scanned twice. The combination of scanners used was different between individuals. In addition, both scanners were simultaneously upgraded during the scan period. However, there was little difference in the Euclidean distances among the different combinations of scanners used or between the probe–gallery image pairs with and without scanner upgrade. This finding is likely to be due to inter-subject variability in brain morphology being much larger than inter-scanner variability and the effect of scanner upgrade. It is generally assumed that inter-scanner variability increases when using scanners of different models and/or manufacturers. We used VBM [7] for image normalization; however, a more sophisticated method of image normalization optimized for brain recognition could possibly suppress the effects of using different scanners and scanner upgrade, even when using scanners of different models and/or manufacturers.

In conclusion, we examined whether brain morphology is personally identifiable information and is discernibly different among individuals (as the basis of individual differences in brain functions), using structural MRI data from 215 healthy subjects who were scanned twice. The results indicate that brain morphology can identify a specific individual; i.e., brain morphology is personally identifiable information. The use of different scanners and scanner upgrade had little effect compared with inter-subject variability in brain morphology.

Acknowledgments

We wish to thank Dr. Eriko Maeda and Dr. Takeharu Yoshikawa for their help in collecting data. This work was supported by a Grant-in-Aid for Young Scientists (A) 24689047 and a Grant-in-Aid for Scientific Research on Innovative Areas 221S0003 (Comprehensive Brain Science Network) from the Japan Society for the Promotion of Science.

References

[1] Maguire EA, Gadian DG, Johnsrude IS, Good CD, Ashburner J, Frackowiak RS, et al. Navigation-related structural change in the hippocampi of taxi drivers. Proc Natl Acad Sci U S A 2000;97(8):4398–403.
[2] Schlaug G, Jancke L, Huang Y, Steinmetz H. In vivo evidence of structural brain asymmetry in musicians. Science 1995;267(5198):699–701.
[3] Munte TF, Altenmuller E, Jancke L. The musician's brain as a model of neuroplasticity. Nat Rev Neurosci 2002;3(6):473–8.
[4] Aydin K, Ucar A, Oguz KK, Okur OO, Agayev A, Unal Z, et al. Increased gray matter density in the parietal cortex of mathematicians: a voxel-based morphometry study. AJNR Am J Neuroradiol 2007;28(10):1859–64.
[5] Mechelli A, Crinion JT, Noppeney U, O'Doherty J, Ashburner J, Frackowiak RS, et al. Neurolinguistics: structural plasticity in the bilingual brain. Nature 2004;431(7010):757.
[6] Draganski B, Gaser C, Busch V, Schuierer G, Bogdahn U, May A. Neuroplasticity: changes in grey matter induced by training. Nature 2004;427(6972):311–2.
[7] Ashburner J, Friston KJ. Voxel-based morphometry—the methods. Neuroimage 2000;11(6 Pt 1):805–21.
[8] Jack Jr CR, Bernstein MA, Borowski BJ, Gunter JL, Fox NC, Thompson PM, et al. Update on the magnetic resonance imaging core of the Alzheimer's disease neuroimaging initiative. Alzheimers Dement 2010;6(3):212–20.
[9] Van Essen DC, Smith SM, Barch DM, Behrens TE, Yacoub E, Ugurbil K. The WU-Minn Human Connectome Project: an overview. Neuroimage 2013;80:62–79.
[10] Ashburner J, Friston KJ. Unified segmentation. Neuroimage 2005;26(3):839–51.
[11] Takao H, Hayashi N, Ohtomo K. Effects of the use of multiple scanners and of scanner upgrade in longitudinal voxel-based morphometry studies. J Magn Reson Imaging 2013;38(5):1283–91.
[12] Fazekas F, Chawluk JB, Alavi A, Hurtig HI, Zimmerman RA. MR signal abnormalities at 1.5 T in Alzheimer's dementia and normal aging. AJR Am J Roentgenol 1987;149(2):351–6.
[13] Jovicich J, Czanner S, Greve D, Haley E, van der Kouwe A, Gollub R, et al. Reliability in multi-site structural MRI studies: effects of gradient non-linearity correction on phantom and human data. Neuroimage 2006;30(2):436–43.
[14] Takao H, Abe O, Hayashi N, Kabasawa H, Ohtomo K. Effects of gradient non-linearity correction and intensity non-uniformity correction in longitudinal studies using structural image evaluation using normalization of atrophy (SIENA). J Magn Reson Imaging 2010;32(2):489–92.
[15] Takao H, Abe O, Ohtomo K. Computational analysis of cerebral cortex. Neuroradiology 2010;52(8):691–8.
[16] Sled JG, Zijdenbos AP, Evans AC. A nonparametric method for automatic correction of intensity nonuniformity in MRI data. IEEE Trans Med Imaging 1998;17(1):87–97.
[17] Good CD, Johnsrude IS, Ashburner J, Henson RN, Friston KJ, Frackowiak RS. A voxel-based morphometric study of ageing in 465 normal adult human brains. Neuroimage 2001;14(1 Pt 1):21–36.
[18] Aloui K, Nait-Ali A, Naceur MS. A novel approach based brain biometrics: some preliminary results for individual identification. Computational Intelligence in Biometrics and Identity Management (CIBIM), 2011 IEEE Workshop on; 2011. p. 91–5.
[19] Aloui K, Nait-Ali A, Naceur MS. New biometric approach based on geometrical human brain patterns recognition: some preliminary results. Visual Information Processing (EUVIP), 2011 3rd European Workshop on; 2011. p. 258–63.
[20] Chen F, Su L, Liu Y, Hu D. Confirming the diversity of the brain after normalization: an approach based on identity authentication. PLoS One 2013;8(1):e54328.
[21] Marcus DS, Fotenos AF, Csernansky JG, Morris JC, Buckner RL. Open access series of imaging studies: longitudinal MRI data in nondemented and demented older adults. J Cogn Neurosci 2010;22(12):2677–84.
[22] Marcus DS, Wang TH, Parker J, Csernansky JG, Morris JC, Buckner RL. Open Access Series of Imaging Studies (OASIS): cross-sectional MRI data in young, middle aged, nondemented, and demented older adults. J Cogn Neurosci 2007;19(9):1498–507.
[23] Takao H, Hayashi N, Ohtomo K. A longitudinal study of brain volume changes in normal aging. Eur J Radiol 2012;81(10):2801–4.
[24] Fjell AM, Walhovd KB, Fennema-Notestine C, McEvoy LK, Hagler DJ, Holland D, et al. One-year brain atrophy evident in healthy aging. J Neurosci 2009;29(48):15223–31.
[25] Kruggel F, Turner J, Muftuler LT. Impact of scanner hardware and imaging protocol on image quality and compartment volume precision in the ADNI cohort. Neuroimage 2010;49(3):2123–33.
[26] Huppertz HJ, Kroll-Seger J, Kloppel S, Ganz RE, Kassubek J. Intra- and interscanner variability of automated voxel-based volumetry based on a 3D probabilistic atlas of human cerebral structures. Neuroimage 2010;49(3):2216–24.
[27] Jovicich J, Czanner S, Han X, Salat D, van der Kouwe A, Quinn B, et al. MRI-derived measurements of human subcortical, ventricular and intracranial brain volumes: reliability effects of scan sessions, acquisition sequences, data analyses, scanner upgrade, scanner vendors and field strengths. Neuroimage 2009;46(1):177–92.
[28] Pardoe H, Pell GS, Abbott DF, Berg AT, Jackson GD. Multi-site voxel-based morphometry: methods and a feasibility demonstration with childhood absence epilepsy. Neuroimage 2008;42(2):611–6.
[29] Stonnington CM, Tan G, Kloppel S, Chu C, Draganski B, Jack Jr CR, et al. Interpreting scan data acquired from multiple scanners: a study with Alzheimer's disease. Neuroimage 2008;39(3):1180–5.
[30] Dickerson BC, Fenstermacher E, Salat DH, Wolk DA, Maguire RP, Desikan R, et al. Detection of cortical thickness correlates of cognitive performance: reliability across MRI scan sessions, scanners, and field strengths. Neuroimage 2008;39(1):10–8.
[31] Han X, Jovicich J, Salat D, van der Kouwe A, Quinn B, Czanner S, et al. Reliability of MRI-derived measurements of human cerebral cortical thickness: the effects of field strength, scanner upgrade and manufacturer. Neuroimage 2006;32(1):180–94.
[32] Ewers M, Teipel SJ, Dietrich O, Schonberg SO, Jessen F, Heun R, et al. Multicenter assessment of reliability of cranial MRI. Neurobiol Aging 2006;27(8):1051–9.
[33] Schnack HG, van Haren NE, Hulshoff Pol HE, Picchioni M, Weisbrod M, Sauer H, et al. Reliability of brain volumes from multicenter MRI acquisition: a calibration study. Hum Brain Mapp 2004;22(4):312–20.
[34] Focke NK, Helms G, Kaspar S, Diederich C, Toth V, Dechent P, et al. Multi-site voxel-based morphometry—not quite there yet. Neuroimage 2011;56(3):1164–70.
[35] Takao H, Hayashi N, Ohtomo K. Effect of scanner in longitudinal studies of brain volume changes. J Magn Reson Imaging 2011;34(2):438–44.
[36] Shuter B, Yeh IB, Graham S, Au C, Wang SC. Reproducibility of brain tissue volumes in longitudinal studies: effects of changes in signal-to-noise ratio and scanner software. Neuroimage 2008;41(2):371–9.
[37] Takao H, Hayashi N, Ohtomo K. Effects of study design in multi-scanner voxel-based morphometry studies. Neuroimage 2014;84:133–40.
[38] Suckling J, Barnes A, Job D, Brenan D, Lymer K, Dazzan P, et al. Power calculations for multicenter imaging studies controlled by the false discovery rate. Hum Brain Mapp 2010;31(8):1183–95.
[39] Vovk U, Pernus F, Likar B. A review of methods for correction of intensity inhomogeneity in MRI. IEEE Trans Med Imaging 2007;26(3):405–21.